Characterization of the planar differential mobility analyzer (DMA P5): 5) : resolving power, transmission efficiency and its application to atmospheric relevant cluster measurements

Zhengning Xu[1], Jian Gao[1], Zhuanghao Xu[1], Michel Attoui[3], Xiangyu Pei[1], Mario Amo-González[4], Kewei Zhang[1], Zhibin Wang[1,2*]

[1]Zhejiang Provincial Key Laboratory of Organic Pollution Process and Control, MOE Key Laboratory of Environment Remediation and Ecological Health, College of Environmental and Resource Sciences, Zhejiang University, Hangzhou 310058, China
[2]ZJU-Hangzhou Global Scientific and Technological Innovation Center, Zhejiang University, Hangzhou 311215, China
[3]University Paris-Est Creteil, University Paris-Diderot, LISA, UMR CNRS 7583, France
[4]MION S.L., Avda. Francisco Valles 8, Boecillo, Valladolid, 47151, Spain

Correspondence to: Zhibin Wang (wangzhibin@zju.edu.cn)

Abstract. The newly developed planar differential mobility analyzer (DMA) serving as particle sizer can achieve higher transmission and selection precision at ambient pressure compared with conventional cylindrical DMA, and show potentials on coupling with atmospheric pressure interface mass spectrometer (API-MS) for cluster detection with an additional ion mobility dimension. In this study, we assessed the performance of a commercial planar DMA (DMA P5) integrated with the home-build recirculation system. The sizing range of the system in this work is 0 sub-3.9 nm, although larger sizes can be measured with a sheath gas flow restrictor. The resolving power under different recirculation setups (suction mode and counterflow mode) and different sheath flow rates was evaluated using electrosprayed tetra-alkyl ammonium salts (TMAI, TBAI, THAB and TDAB). The maximum resolving power of THA^+ under suction and counterflow mode are 61.6 and 84.6, respectively. The sizing resolution of DMA P5 is 75-16 times higher than conventional cylindrical DMAs. The resolving power showed approximately linear correlation with $\sqrt{V_{DMA}}$ under counterflow mode, while the resolving power of THA^+ under suction mode stopped linearly increasinge with $\sqrt{V_{DMA}}$ when the V_{DMA} was above 3554.3V and entered a plateau due to the interference of sample flow on the laminarity of sheath flow. The transmission efficiency of DMA P5 can reach 54.3%, about one factor order of magnitude higher than the commercial DMAs. The mobility spectrum of different electrosprayed tetra-alkyl ammonium salts and the mass to charge ratio-mobility 2D spectrum of sulfuric acid clusters was also characterized with the DMA P5 (-MS) system.

1 Introduction

Measurement of the physical and chemical properties of sub-3 nm particles is essential for understanding atmospheric aerosol nucleation mechanisms (Kerminen et al. 2018). Differential mobility analyzer (DMA) has long been used for aerosol sizing

and classifying (Knutson & Whitby, 1975). TSI Nano-DMA (Model 3085, Chen et al., 1998) and TSI 1 nm-DMA (Model 3086, Stolzenburg et al., 2018) were designed for particle sizing down to 3 nm and 1 nm, respectively. Equipped with these DMAs, the ~~newly developed~~ DEG-based scanning mobility particle sizer (SMPS) system (Jiang et al., 2011) can be applied to measure the size distributions of sub-3 nm particles (Cai et al., 2017).

Various mass spectrometry-based approaches have been utilized for measuring the chemical composition of clusters and their precursors (Chen et al., 2020; Peng et al., 2022). However, these approaches lack direct measurement of cluster size and structure. In Thermal Desorption Chemical Ionization Mass Spectrometer (TDCIMS) system (Smith et al., 2004), size resolved particles were separated by DMA(s), and analyzed by mass spectrometry when sufficient particles were accumulated th~~o~~rough electrostatic deposition. Currently, the detect limit of TDCIMS was 5 nm (Perraud et al., 2020). For cluster study, a much longer accumulation period is needed, due to the drastic decrease of charging efficiency with decreased particle diameter and low ion transmission of the applied DMAs. DMAs coupled directly to mass spectrometer (DMA-MS) can achieve spontaneous detection of ion mobility and chemical composition, and can serve as a promising tool to study the physicochemical properties of atmospheric clusters and the formation mechanism of particle nucleation and initial growth (Zhang et al., 2022). The performance of the applied DMA on sizing sub-3 nm particles is the only limitation of this technique.

Planar DMAs have been successfully coupled to several commercial atmospheric pressure interface mass spectrometer (API-MS) under high resolving power and high transmission (Hogan and Fernandez de la Mora, 2009; 2010; Hogan et al., 2011; Criado-Hidalgo et al., 2013). The physicochemical properties of various atmospheric clusters such as metal iodide clusters (Oberreit et al., 2014; Oberreit et al., 2015), dimethylamine (DMA) and sulfuric acid complexes (Ouyang et al., 2015; Thomas et al., 2016), sodium chloride clusters (Li and Hogan, 2017) and hybrid iodine pentoxide–iodic acid clusters (Ahonen et al., 2019) were investigated by DMA-MS. Rus et al. (2010) have characterized several prototypes of planar DMAs and the transmission of DMA P4 was ~50%. On the basis of DMA P4, DMA P5 updated the design of outlet, guaranteeing that the assemble/disassemble of DMA to/from MS would not break the vacuum (Amo-González and Pérez, 2018).

To our knowledge, the characterization of commercial DMA P5 have not been reported. In this work, the performance of DMA P5 under different working conditions ~~with a home-build recirculation circuit~~ was characterized. The resolving power and transmission efficiency were characterized using standard ion clusters. The DMA P5 was also deployed to measure the ion mobility spectrum of electrosprayed clusters of different tetra-alkyl ammonium salts and the mass to charge ratio-ion mobility 2D spectrum of sulfuric acid.

2 Experimental setup and methodology

In this study, DMA P5 (SEADM, Valladolid, Spain) was used, which consisted of a pair of plate parallel ~~electrodes~~ plates separated by insulated holders. The combination of horizontal laminar sheath flow and vertical electric field between the separation region of the two electrodes acts a spatial mobility filter (Purves et al., 1998). Polydispersed aerosols penetrating through inlet slit at the inlet electrode move toward the outlet electrode under the electric field force. For a fixed sheath flow

velocity and electric field pair, monodispersed aerosols with super narrow ion mobility range can penetrate through the outlet hole at the outlet electrode and transmit to the detectors. The detailed design and critical dimensions of DMA P5 has been described by Amo-González and Pérez (2018). The theoretical principle of planar DMA on particle sizing is described in SI (Section 1). The ion mobility of selection can be estimated by the following the formula:

$$Z = \frac{U \cdot h^2}{L \cdot V_{DMA}} \qquad (1)$$

where Z represents the ion mobility of selection, U represents the velocity of sheath flow in the symmetry plane going through the center of the inlet slit, h represents the distance of the two electrodes, L represents the horizontal distance between inlet slit and outlet hole, V_{DMA} represents the voltage difference between the two electrodes.

The ~~home made~~ recirculation circuit needed for DMA P5 system ~~was adapted,~~ should be able to provid~~e~~ing particle free sheath flow with stable velocity and temperature. The recirculation circuit deployed in this study consists of air blower (Ref 497.3.265-361, Domel), ~~home build~~ water cooler coupled with constant temperature water bath (DCW-2008, SCIENTZ), particle filter adapted for high flow velocity, ~~particle filter (Ref 34230010, Megalem MD143P3, Camfil Farr) adapted for high flow velocity,~~ NW40 and NW 50 corrugated stainless-steel tubes and connectors. The particle filter consists a planar commercial HEPA filter (Ref 34230010, Megalem MD143P3, Camfil Farr) and two stainless assembly. The top side of the assembly is a NW40 connector, while the bottom side fits the geometry of the planar HEPA filter. The HEPA filter is sandwiched between the two bottom surfaces of the assembly, sealed with O-ring and screws. All the components are purchased from the local market. Alternative products with similar performance should not affect the operation of the whole system. The rotational speed of the blower was controlled by 0-10 Vdc analogue signal (V_{blower}). The flow rate under different control voltage was calculated by Eq. (1) using the ion mobility and V_{DMA} of standard ion (THA^+) (Fig.S2). The temperature was controlled to be 24 Celsius degrees.

The nano-ESI ionization source (SEADM, Valladolid, Spain) was adapted. The main body of the nano-ESI ionization source is a PEEK cubic electrospray chamber, assembled with the inlet electrode of DMA P5 on its bottom, sealed on front and back ends by two glass windows, coupled with 1/8" capillary guide on the top middle. There were another two 1/4" ports for flow injection and exhaust on the top left and right of the ionization chamber.

In this study, two types of recirculation circuit setup (suction mode and counter flow mode) were characterized based on the design of ionization source. Under suction mode, aerosols were transport to the inlet slit by the combination of the electric field between the electrospray and the DMA inlet electrode and the polydisersed aerosol flow (Q_{in}) and sucked into the separation region under the monodispersed aerosol flow (Q_{out}), the excess flow (Q_{excess}) was exhausted from another port. Under counter flow mode, only one port was used to exhaust the counter flow (Q_{count}) out of the inlet slit. Compensate flow (Q_c), with the flow rate equal to the sum of Q_{count} and Q_{out}, was introduced into the circuit th~~e~~rough a T connector. The detailed recirculation circuit setups are illustrated in Fig. 1.

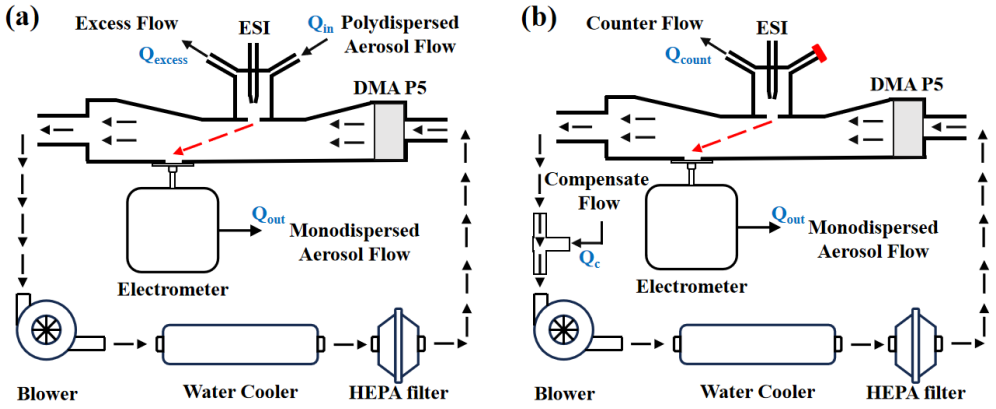

Fig.1 Schematic diagram of the recirculation circuit setups (a) suction mode; (b) counter flow mode of DMA P5 system.

The performance of the DMA P5 was characterized by classifying aerosols generated via electrospraying of salt solutions. A silica capillary (FS360-50-N-5-C50, New Objective) fitted in the capillary guide of nano-ESI ionization source was applied to connect the ionization chamber and the vial of solution. The connections on both ends of the capillary were established with standard capillary connections used for liquid chromatography. The vial was connected to a pressure sensor and a syringe equipped with a valve th~~e~~rough a T-connector. The solution was pushed through the capillary by compressing the gas inside the vial until the desired pressure above the solution surface was achieved. The valve in front of the syringe~~springer~~ was then turned off, keeping the pressure constant for a long period. High voltage was applied to the solution through an inert metal wire immersed in it. Similar methodologies have been proposed by Jiang et al. (2011) and Cai et al. (2018). With positive voltage applied and without subsequent neutralization, singly charged, positive polarity aerosols can be generated (Ude and Fernández de la Mora 2005). In this study, pressure (P_{ES}) and voltage (V_{ES}) of the electrospray source were set to ~20 kPa and ~2000 V, respectively. The Faraday cage electrometers (Lynx E11&E12, SEADM, Valladolid, Spain, Fernandez de la Mora et al., 2017) ~~was~~ were used as particle counter. The output signal range was 0-2V, with an amplification of 10^{11} V/A and 10^{12} V/A, respectively. Based on Eq. (1), the ion mobility of any aerosols with known DMA voltage can be calibrated with standard ions under constant sheath flow velocity by the following formula:

$$Z = \frac{V_{standard} * Z_{standard}}{V_{DMA}} \qquad (2)$$

where $Z_{standard}$ represents the electric mobility of standard ion, V_{DMA} and $V_{standard}$ represent the DMA voltage of target aerosol and standard ion under the same sheath flow rate. Standard ion (THA^+), with the known mobility of 0.97 $cm^2\ V^{-1}\ s^{-1}$ (Ude and Fernández de la Mora 2005), was generated via positive electrospraying of 0.5 mM THABr solution in 9:1 methanol/water mixture. The mobility diameter in this manuscript is calculated with the Stokes-Cunningham equation (Tammet, 1995; Wiedensohler et al., 2012). Detailed information about the mobility diameter calculation is described in SI (Section 2). The sizing range under different rotational speed was calculated using Eq. (2), given the upper VDMA limit of 10 kV. The sizing

upper limit of DMA P5 in the current configuration was 1.9-3.9 nm, although using a flow restrictor in the sheath gas circuit the upper size can be extended. Higher sheath flow rate corresponded to lower sizing range (Fig. S2).

The sizing resolution of specific aerosol (R) is defined as the ratio of the central electrical mobility (Z) and the full width at half maximum for the peak (ΔZ_{FWHM}) (Flagan 1999):

$$R=\frac{Z}{\Delta Z_{FWHM}} \quad (3)$$

The theoretical calculation of planar DMA sizing resolution is given by the following equation (Amo-González and Pérez, 2018 and SI Section 3 for detailed derivation process):

$$R^{-1}=\frac{\Delta L_{0.5}\Delta Z_{FWHM}}{LZ}=\sqrt{\left[\left(\frac{Q_{in}+Q_{out}}{L_{slit}2\,Re\,v}\right)^2+\frac{16ln2kT}{V_{DMA}N_e}\left(1+\left[\frac{h}{L}\right]^2\right)\right]} \quad (4)$$

where, Q_{in} represent the polydispersed aerosol flow rate and Q_{out} is the monodispersed aerosol flow rate, respectively, L_{slit} is the length of inlet slit, Re is the Reynolds number, v is the viscosity of the sheath gas, k is the Boltzmann's constant, T is the absolute temperature of the sheath gas, Ne is the net charge on the aerosol.

3 Results and Discussion

3.1 Resolving Power under different recirculation modes

The key point of applying ESI source with DMA P5 is that the ESI voltage is not constant under scan mode. The voltage applied to the nano-ESI source floats above the inlet electrode voltage of DMA P5 with the floating value being the exact ESI voltage. Such configuration can avoid the influence of the voltage change during the scan~~ning~~ mode on the formation and stability of electrospray. Moreover, the electric field between the capillary tip and the inlet electrode guides the aerosol into the DMA separation chamber. According to such design, as being illustrated in the former section, two recirculation modes can be applied for DMA P5 operation for characterizing its performance with standard aerosol generated from nano-ESI source. Under suction mode, polydispersed aerosols are sucked into the DMA separation region. Under counter flow mode, the aerosols are inserted electrically into the DMA, the inlet slit counter flow accelerates the evaporation of droplets and prevent the neutral droplets from entering the DMA separation region.

Based on Eq. (4), large Re is expected in order to achieve high sizing resolution, under which condition the sheath flow velocity needs to be very large based on the following equation:

$$Re=\frac{Uh}{v} \quad (5)$$

Suction of aerosol sample can easily disturb the sheath flow, and decrease the sizing resolution. Moreover, incomplete desolvation of solvent and entrance of neutral droplet into the DMA separation region under suction mode may also affect the peak shape, obscuring the identification of analytes of interest (Amo-González and Fernández de la Mora, 2017). On the other hand, suction mode can obtain higher aerosol number concentration at the expense of resolving power and peak shape.

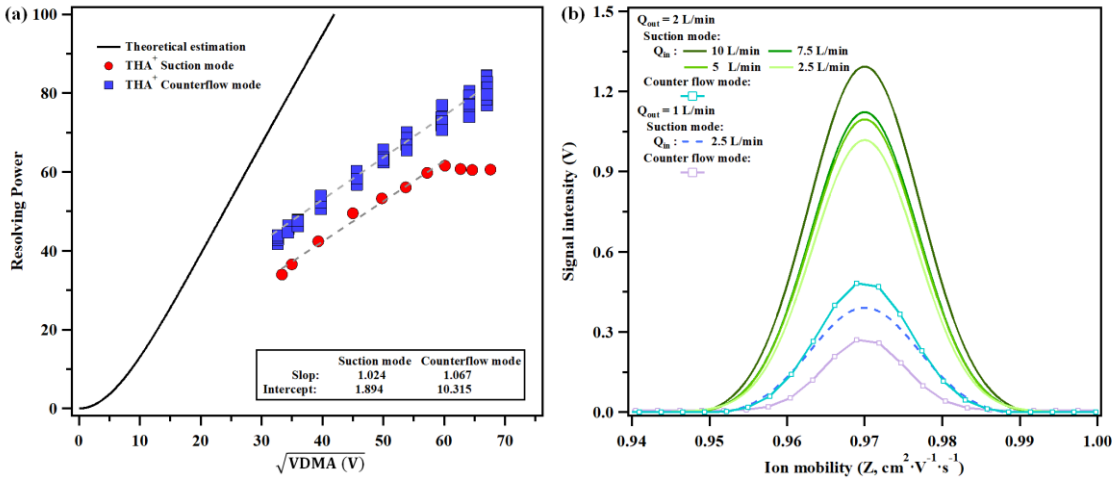

Fig 2. (a) The dependency of the resolving power of THA^+ on DMA voltage (V_{DMA}) under suction mode and counter flow mode; (b) dependency of the resolving power and signal intensity on the Q_{out} under suction mode and the comparison with counterflow mode.

According to Eq. (1), V_{DMA} is approximately linearly correlated with the sheath gas velocity under fixed ion mobility. According to Eq. (4), R increases with the increase of $\sqrt{V_{DMA}}$ with determined DMA physical structure (h, L), sheath flow properties (v, T, U) and aerosol charge state (Ne). The performance of DMA P5 for obtaining the THA^+ mobility spectrum under suction mode is shown in Figure S3. With solution concentration higher than 0.5mM, well separated THA^+ monomer, dimer and trimer can be observed. Hihger solution concentration leads to the increase of the signal/noise ratio, but decreases the dimer/monomer ratio. As can be derived from Eq. (1) and Eq. (4), both the V_{DMA} and corresponding sizing resolution of THA^+ increases with the increase of sheath flow rate. Figure 2a shows the dependency of the resolving power of sizing 1.47 nm ions (THA^+) on $\sqrt{V_{DMA}}$ under two recirculation modes by changing the sheath flow velocity. ~~Q_{out} is 2 L/min under the two recirculation modes.~~ Q_{in} is 5 L/min under suction mode. $Q_{counter}$ is 0.5 L/min under counter flow mode.

Under suction mode, R showed positive linear correlation with $\sqrt{V_{DMA}}$, with the slope and intercept of 1.024 and 1.894, respectively, when the V_{DMA} was below 3554.3V. R remained nearly unchanged with the increase of $\sqrt{V_{DMA}}$, when the V_{DMA} was above 3554.3V. In high V_{DMA} range (corresponding to higher sheath flow velocity), R was in the range of 60 ± 3. Under counter flow mode, R and $\sqrt{V_{DMA}}$ showed good linear relationship (R^2=0.95) within the sheath flow velocity range of the applied system. The slope and intercept of 1.067 and 10.315, respectively.

Generally, the resolving power of THA^+ was higher under counter flow mode, and was ~~much~~ significantly closer to the theoretical calculation. With the increase of the sheath flow velocity, the difference between the measurement and the theoretical calculation gradually increased. Under the suction mode, due to the interference of polydispersed sample flow, the resolving power was 14.9%-21.7% lower than that of the counter flow mode when $\sqrt{V_{DMA}}$ was lower than 59.6. The discrepancy increased to 24.9 % when $\sqrt{V_{DMA}}$ reached 66.0. The reason for the difference of resolving power between the two

recirculation modes and the deviation from the theoretical calculation is the turbulence effect. The higher the sheath flow rate velocity is, the easier for the flow to become turbulent, consistent with the measurement result that the resolving power stopped increasing when V_{DMA} was over 3554.3V. The increasing discrepancy of measured and theoretical resolving power was attributed to the insufficient stabilization of sheath flow to the laminar condition. Adding an additional pair of prelaminarizer screens into the sheath flow recirculation circuit under counter flow mode can increase the resolving power approaching it to the theoretical limit (Amo-González and Pérez, 2018).

Figure 2b shows the change of THA^+ peak signal intensity and resolving power to different Q_{in} under suction mode. The change of Q_{in} showed little effect on resolving power (58.06-61.58, with the relative deviation being -3.5%-2.3%), while had significant influence on signal intensity (number concentration of the sizing aerosol). With constant Q_{out} of 2 L/min, the peak signal of THA^+ is 1.31 V, 1.13 V, 1.1 V and 1.02 V, under Q_{in} of 10 L/min, 7.5 L/min, 5 L/min and 2.5 L/min, respectively. When Q_{out} was decreased to 1.0 L/min, the signal strength was significantly reduced. It should also be noted that at the cost of the decreased resolving power, higher signal intensity of electrometer was obtained under suction mode. The peak signal of THA^+ under suction mode was 108.2%-167.3% higher compared with counter flow mode at the same Q_{out}.

Under the counter flow mode, there are two adjustable parameters, namely counter flow rate (Q_{count}), and monodispersed aerosol flow rate (Q_{out}). Figure 3 shows the influence of Q_{count} and Q_{out} on the sizing resolution and number concentration under the fixed sheath flow rate (about 1200 L/min, under which speed the recirculation system can operate for a long time without increase of temperature). Figure 3a and b show the change of THA^+ central voltage and signal intensity under different Q_{out} at Q_{count} of 0.5 L/min and 1.0 L/min, respectively. In general, the signal strength increased monotonously with the increase of Q_{out}. According to theory (Knutson & Whitby, 1975), the THA^+ central voltage decreased with the increase of Q_{out}. Compared with Q_{count}, Q_{out} had a greater impact on the measurement results. Figure 3c shows the relationship of the integrated peak area of THA^+, the resolving power and the central voltage with Q_{out}. With the increase of Q_{out} from 0.5 L/min to 3.0 L/min, the central voltage of THA^+ decreased by about 20 V (less than 1%); the integrated peak area increased by 7.6 and 6.8 times for Q_{count} of 1.0 L/min and 0.5 L/min, respectively; the resolving power decreased from 75 to 69. We defined the counting efficiency of electrometer as the integrated peak area / Q_{out}. The relation of the counting efficiency with Q_{out} (Fig. ~~S3~~S4) indicated that the counting efficiency would increase with the increase of Q_{out} before reaching 2 L/min and decrease afterward. Setting the total Q_{out} over 2.0 L/min would result in the decreasing of both counting efficiency and resolving power and is not recommended when coupling with an API-MS.

It should also be noted the above-mentioned recirculation set ups are applied for the study of aerosols generated from ESI source. For the measurement of atmospheric clusters, secondary electrospray ionization (SESI) (Rioseras et al., 2017) is applied, with the reagent ions generated via electrospraying of custom selected solutions. Under injection mode, clusters are introduced to the DMA from the polydispersed aerosol flow inlet. Under counter flow mode, the blocked port (red labeled in Fig. 1b) is used to introduce the atmospheric clusters, while the O_{count} is equal to the sum of the counter flow rate and the sample flow rate. Gao et al. (2023) have deployed the SESI-DMA-TOF for the measurement of the products of α-pinene ozonolysis.

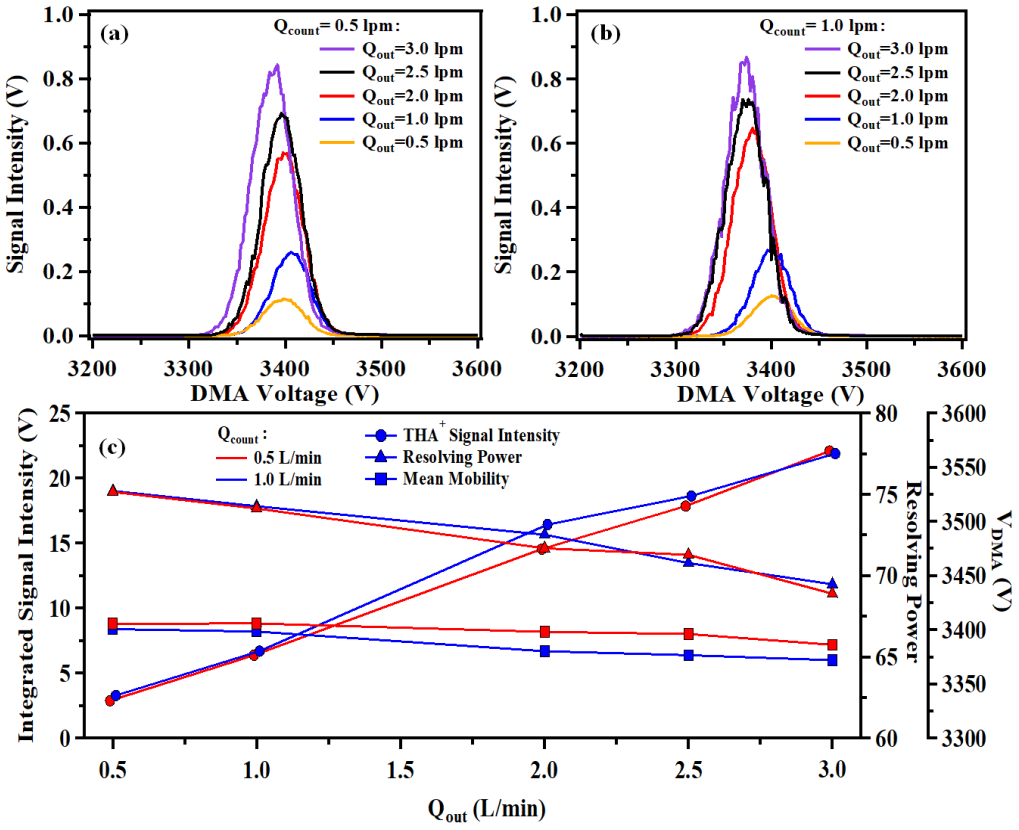

Fig. 3 Mobility spectrum of THA^+ under different Q_{out} with (a) $Q_{counter}$ = 0.5 L/min; (b) $Q_{counter}$ = 1.0 L/min; (c) Integrated signal intensity, resolving power and V_{DMA} of THA^+ under different Q_{out}.

The sizing resolution of THA^+ monomer by DMA P5 and Half Mini DMA (Fernandez de la Mora and Kozlowski, 2013), measured in our lab, were compared with the reported results of different types of commercial DMAs (Jiang et al., 2011, Stolzenburg et al., 2018). The DMA P5 was operated under counter flow mode at the sheath flow rate of about 1500 L/min (corresponding to the V_{blower} of 8.5 V). The Half Mini DMA was operated at the aerosol-to-sheath flow ratio of 10/300 L/min. The reported resolution was measured under the aerosol-to-sheath flow ratio of 0.6/6 L/min for the Caltech nanoRDMA, of 6/61.4 L/min for the Vienna DMA, of 2/21.9 L/min for the Grimm nanoDMA, of 2.0/20 L/min for TSI 3085, of 2.5/25 L/min for TSI 3086 and of 1.5/15 L/min for the Caltech RDMA. The aerosol-to-sheath flow ratio for all reported cylindrical DMAs (except HalfMini DMA) is approximately 10, which is the typical flow configuration for particle sizing in both lab and field measurements. The comparison results show that the planar DMA has the highest sizing resolution, which is ~~7~~5-16 times higher than ~~conventional~~ cylindrical DMAs ~~and 5-6 times higher than Half Mini~~ (Fig. 4). On one hand, due to the high maintaining expenses for keeping the super high sheath flow rate, application of DMA P5 on atmospheric particle number size distribution measurements is unpractical. On the other hand, high resolution and high ion transmission are almost synonymous

for planar DMAs. This advantage is merit of being further exploited by coupling with mass spectrometer for cluster detection with an additional ion mobility dimension. The mobility spectrum of THA^+ obtained from Half Mini is shown in Fig. ~~S4~~S5. The obtained well separated THA^+ ion beam was utilized for characterizing the ion transmission efficiency of DMA P5.

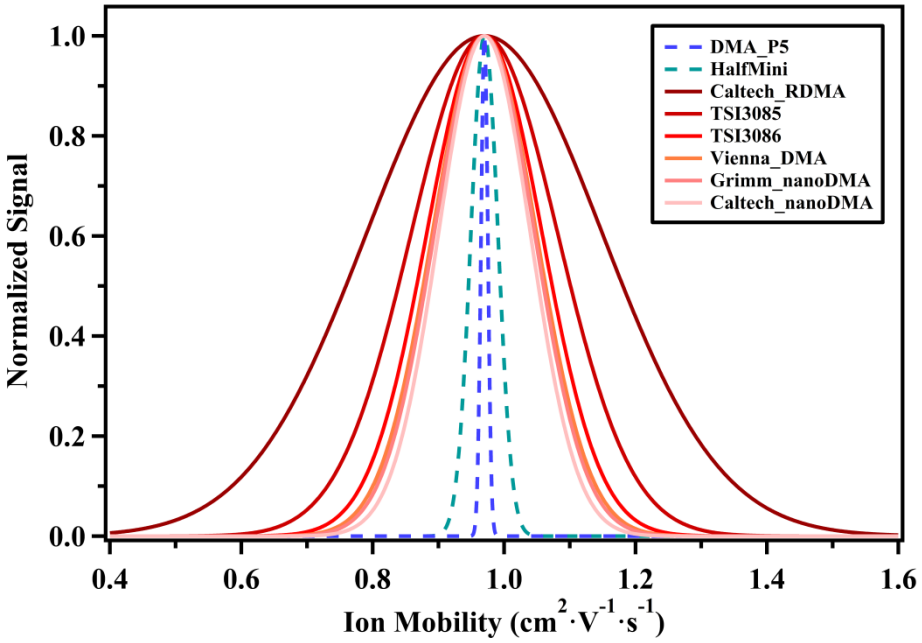

Fig. 4 Comparison of the resolving power of DMA P5 and other commercial DMAs for detecting THA^+. DMA P5 was operated under the sheath flow rate of 1500 L/min, Half Mini was operated under the sheath flow rate of 300 L/min. All the signal intensiy is normalized with the peak height.

In addition to THAB, the sizing ability of DMA P5 was also characterized with three other tetra alkyl ammonium halides (tetra methyl ammonium iodide (TMAI), tetra butyl ammonium iodide (TBAI) and tetra decyl ammonium bromide (TDAB)). The concentration of the solution is 0.5 mM/L. Figure 5 and Figure 6 show the positive and negative ion mobility spectra. The results showed that well defined, single positive charged monomers and dimers can be obtained for the four salt solutions, trimers of TBAI and THAB can also be observed. The negative ions of halogen elements are the main products in the negative ion spectrum. Eq. (2) is used to calculate the mobilities of aerosol ions, and the results are shown in Table S1 and Table S2. The estimated results were consistent with the results reported by Ude et al. (2005).

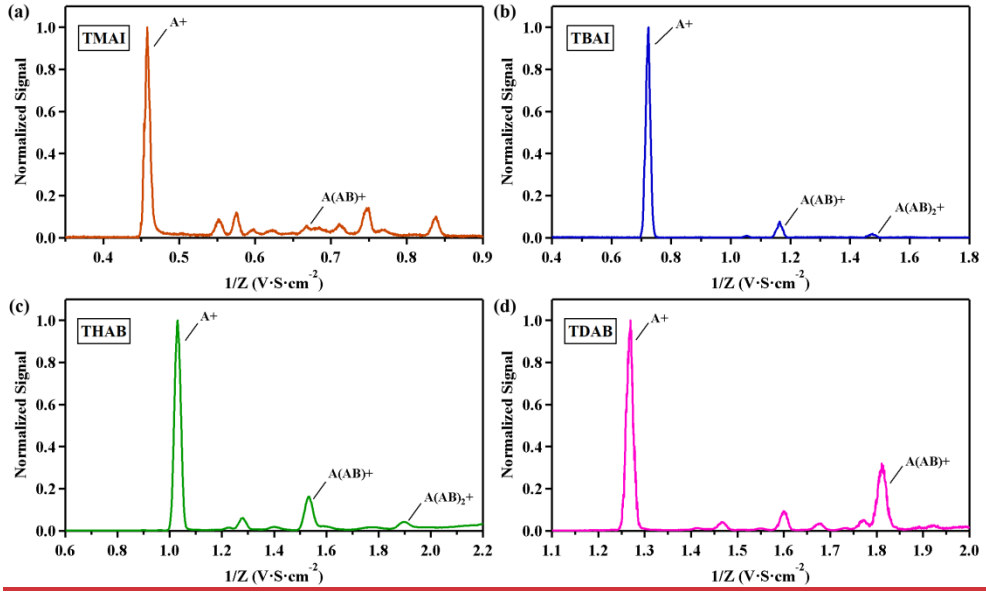

Fig. 5 Positive mobility spectrum of electrosprayed tetra-alkyl ammonium ions, (a) TMAI, (b) TBAI, (c) THAB, (d) TDAB.

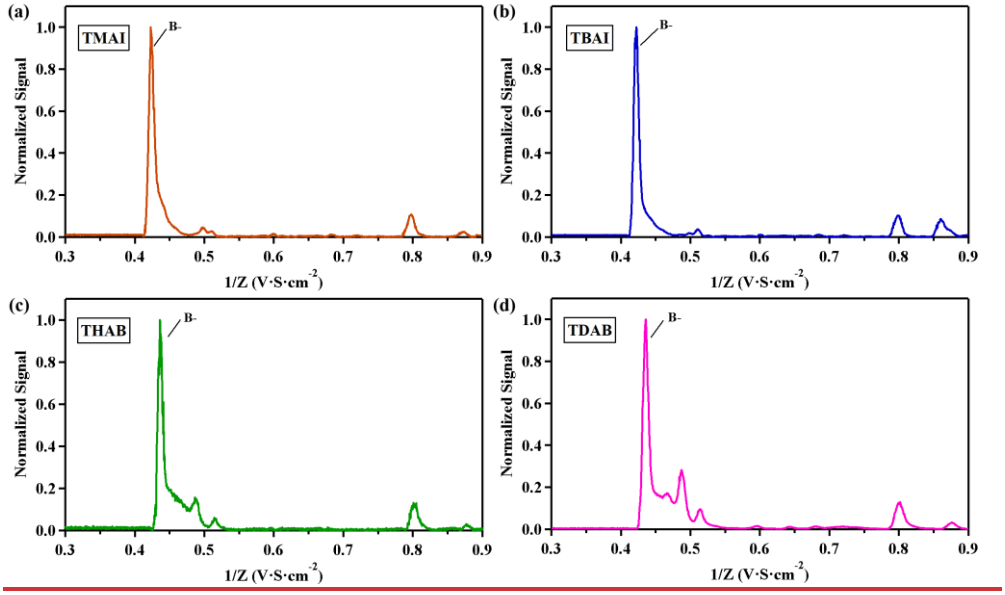

Fig. 6 Negative mobility spectrum of electrosprayed tetra-alkyl ammonium ions, (a) TMAI, (b) TBAI, (c) THAB, (d) TDAB.

According to equation Eq. (4), the resolving power of planar DMA is directly related to V_{DMA} and Ne (net charge of the ions). The relationship between the resolving power of the positive charged monomers of THAB, TMAI, TBAI and TDAB with the V_{DMA} under different sheath flow velocity is shown in Figure 7. The result showed that the resolving power (R) and

$\sqrt{V_{DMA}}$ of different types of tetra alkyl ammonium cations presented an excellent linear relationship (R^2=0.96), with the slope and intercept of 0.992 and 13.511. As illustrated in Fig. 7, most data points were within the 95% confidence interval. This result can be used as the reference for the variation of the resolving power of DMA P5 under the counterflow mode with different sheath flowrate. Moreover, the resolution function can also be used for multi-peak fitting, which can be applied in peak identification of the ion mobility spectrum of multi-component complexes.

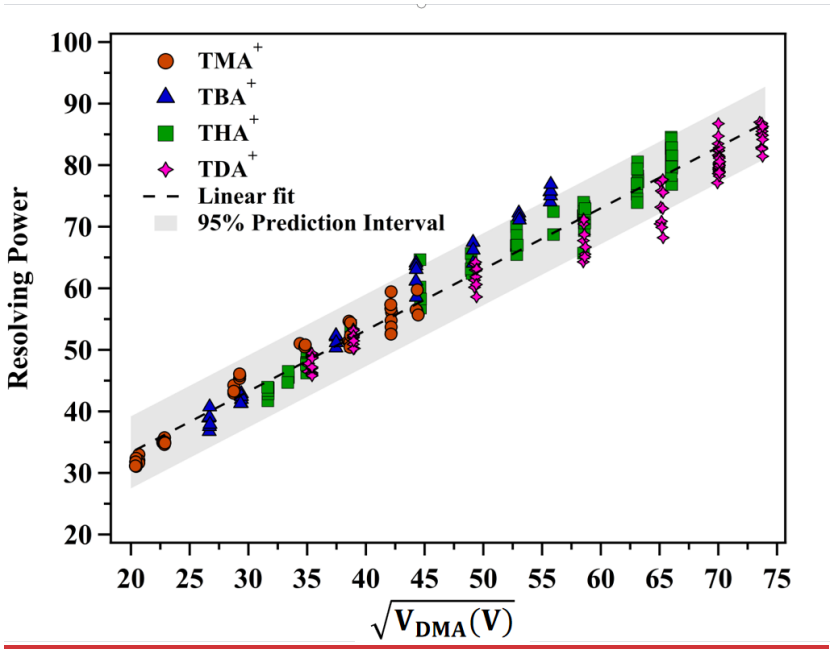

Fig. 7 Relation of resolving power of different cluster ions with V_{DMA}

3.2 Transmission efficiency

The most important issue of applying the DMA P5 for atmospheric cluster studies is whether it can select sufficient amounts of ionized clusters for further analysis at an acceptable time scale. Therefore, the performance of DMA P5, especially the transmission efficiency, needs to be characterized. There are studies with electrospray sources directly facing a planar DMA inlet slit, showing many orders of magnitude gains in transmitted ion signal versus cylindrical DMAs: Javaheri et al. (2008) have shown that almost all molecules of an electrosprayed dilute species in solution can be transmitted as ions to the atmospheric inlet orifice of a mass spectrometer. Similarly, over 1 nA of the dominant electrosprayed ion can be transmitted to the outlet slit of a planar DMA (Fernandez de la Mora, 2019). Such advantage of planar DMA has been exploited by Tauber et al. (2018) to introduce DMA-purified highly concentrated atomic ions into a nucleation chamber to study ion induced nucleation. This exceptional transmission cannot be achieved with any cylindrical DMA, which is the main reason why most successful couplings of DMAs with MS systems (mainly using electrospray sources) have involved planar DMAs. For example,

it took over an hour with a high resolution cylindrical DMA (passing 10 L/min of aerosol) set at a fixed voltage in tandem use with a Time of Flight (TOF) mass spectrometer to accumulate a single mass spectrum with useful information on $(THABr)_n(THA^+)_z$ clusters (Fernandez de la Mora et al. 2005). There are nevertheless exceptions involving quadrupole MS systems set at a fixed mass, while a cylindrical DMA scans over the voltage (Ude et al., 2004). Steiner et al. (2014) have successfully coupled a cylindrical DMA of relatively high resolution to a TOF-MS to investigate small ions from radioactive bipolar sources.

However, an electrospray is an intense unipolar ion source injecting several hundred nA of current into an area typically smaller than $1\mu m^2$. In this case, the major source of ion loss is beam broadening by space charge, which would not be relevant in most atmospheric measurements. The transmission efficiency of DMA P5 in this study was characterized using a tandem DMA system (Fig. S6). Most of electrospray ions are lost by space charge in the aerosol inlet tube and in the annular region preceding the inlet slit to the analyzing region of the first DMA. Consequently, there is little space charge left when these ions reach the second DMA. Therefore, the losses measured are primarily diffusive losses, which is what would be relevant in atmospheric sampling. A Half Mini DMA operated at fixed sheath flow and voltage was applied as the upstream DMA selecting only THA^+ monomer. Such configuration can also minimize the influence of multi-charged ions with larger molecular weights (Attoui et al., 2013).

Standard aerosol ions (THA^+) were generated following the same method described above. To verify that the upstream DMA carried only THA^+ monomer, before each experiment, a full mobility spectrum was taken under voltage scanning mode and compared with published result (Liu et al., 2021). Lynx E11 and E12, with amplifications of $1x10^{11}$ and $1x10^{12}$ V/A, respectively, were used to measure the aerosol number concentration upstream and downstream of the DMA P5. An additional experiment connecting the two electrometers to the Half Mini DMA th~~e~~rough a flow splitter (TSI 3780) with the same tube length was conducted to determine the correction factor. The Half Mini DMA was operated under fixed voltage, selecting only THA^+ ions. The sample flow rates of the electrometers were measured using a bubble flowmeter. The signal of the two electrometers was measured simultaneously. The correction factor of the two electrometers was 10.34, which ~~it~~ is quite close to the theoretical amplification relation of the two electrometers. In order to correct the ion loss to the tube wall, the tube length between the flow splitter (TSI 3780) and the electrometers (excluding the DMA P5) were identical.

Downstream to the Half Mini DMA, DMA P5 was connected between the flow splitter and the second electrometer. A 3D-printed cubic chamber was used to connect the inlet tube and DMA inlet slit. The inner geometry of cubic chamber was cylinder-shaped, with the diameter of 32 mm, and the height of 6.5 mm. The inlet tube was inserted straightly into the centre of the cylinder-shaped space thorough the hole on the top of the cubic chamber. The space between the conductive silicone tube and the hole was sealed with silicone glue. The injection end of the inlet tube was connected to the beam splitter, while the exit end was at the same surface with the lower end of the chamber. When the cubic chamber was sealed to the inlet electrode of DMA P5, the distance between the exit end of inlet tube and the inlet slit of DMA P5 is about 5.2 mm. During the experiments, the voltage for Half Mini DMA was fixed and the voltage for the DMA P5 was scanned continuously. The ion

number concentration recorded by the two electrometers was~~Ion transmission efficiency was equal to the ratio between the ion number concentrations measured by the downstream and upstream electrometer, both~~ given by the following equation:

$$N = V_{EM}/(amp \cdot e \cdot q) \qquad (6)$$

where V_{EM} represent the signal of electrometer, *amp* is the amplification coefficient of the electrometer, q is the sample flow rate of electrometer and e represents elementary charge. The recorded concentration was then corrected using the correction factor.

DMA P5 was operated under suction mode with inlet electrode grounded, and outlet electrode connected to the negative voltage. The grounded downstream electrometer was connected to outlet electrode with a straight 10 cm dissipative plastic tube (85A, FreelinWade, Oregon) (Attoui et al., 2016). The dissipative plastic tube was the key component of the experimental setup, which can avoid electrostatic accumulation on the inner tube surface. The dissipative plastic tube was kept straight, connecting to the outlet electrode and downstream electrometer in good electrical contact. Counter flow mode was not tested due to the difficulty to control the electric field needed for conventional positive voltage setting (inlet electrode connected to positive voltage, and outlet electrode grounded) to push the ions against the counter flow with the presence of the sample tube. These experiments were carried out under different sheath flow velocity (corresponding to different control voltage, Fig. S2).

The transmission illustrated is the maximum transmission efficiency, which is defined as the peak height of the ratio of the aerosol number counted by the downstream and upstream electrometer (N_{down}/N_{up}). The experimental results of N_{down}/N_{up} under different working condition is shown in Fig. S7 and S8. The transmission efficiency as the function of Q_{out} are shown in Fig. ~~5a~~8a. The transmission efficiency showed linearly correlation with increased Q_{out}. The highest ion transmission was 54.3% under the highest Q_{out} (3 L/min) and the lowest sheath flow velocity. Under the above-mentioned configuration, electric field between outlet electrode with a high negative voltage and the grounded electrometer will drag THA^+ ions back to the DMA outlet constantly. Sufficient ~~Q_{in}~~ Q_{out} is called to compensate the electrical velocity. As depicted by Eq (1), higher V_{DMA} is needed for selecting particle with the same mobility under higher sheath flow velocity. With increasing sheath flow velocity, the ion transmission efficiency decreased due to insufficient compensation of electrical velocity. It should be noted that under conventional DMA P5 configuration (both outlet electrode and detectors are grounded), the ion loss due to the electrical dragging force is negligible. Thus, the transmission efficiency is no longer related to the Q_{out}. Consequently, our results represented the lower limit of the DMA P5 ion transmission. The ion transmission of TSI 1 nm-DMA (Model 3086) was also characterized with the same TDMA system. The ion transmission was 4.7% and 7.1% for sheath/ sample flow ratio of 25 L/min /2.5 L/min and 30 L/min / 3.0 L/min, respectively. DMA P5 illustrated 4.5-17.5 times higher ion transmission efficiency compared with other cylindrical DMAs (Fig. ~~5b~~8b).

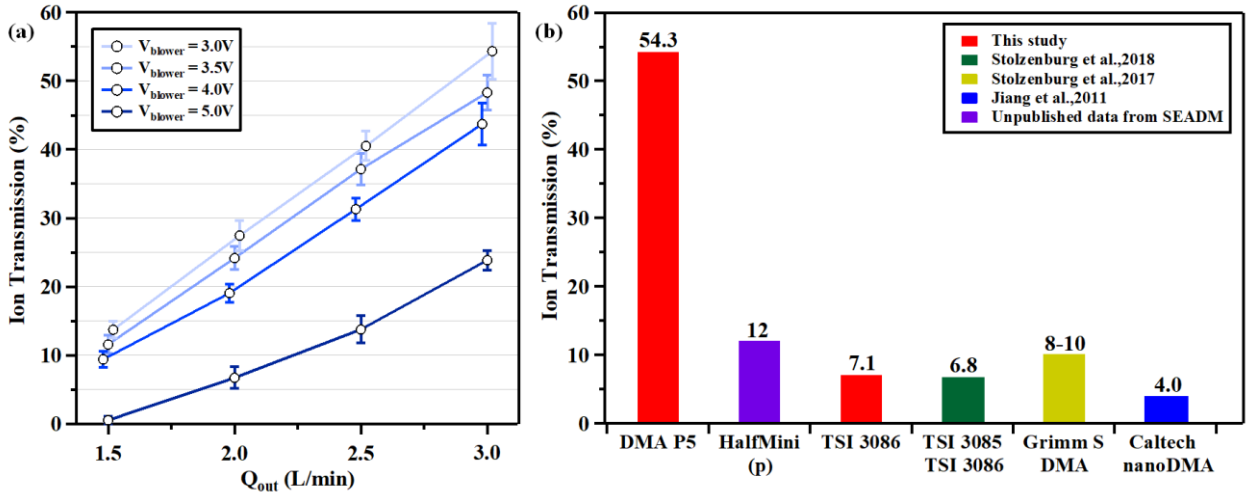

Fig. ~~5~~ 8 (a) Ion transmission efficiency of P5 under different Q_{out}; (b) Comparison with other cylindrical DMAs (the red bars represent the experimental results).

3.3 Applications ~~on aerosol sizing and~~of DMA P5 by coupling with mass spectrometer

There are excellent commercial instruments able to measure both mobility and mass in tandem（ion mobility spectrometry-mass spectrometer, IMS-MS）. Most of them use either intense potentially fragmenting electric fields in the mobility analyzer, or carry the mobility analysis in a region of reduced pressure (May and McLean, 2015). What is special about the DMA P5 is that it operates at atmospheric pressure and has little tendency to fragment even weakly bound clusters, which is very suitable for the detection of atmospheric clusters. Sulfuric acid molecules and clusters, as important participants of new particle formation (Kulmala et al., 2000), were chosen to evaluate the performance of DMA P5 as an ion mobility filter for the study of atmospheric relevant clusters. The experimental set-up consisted of the nano-ESI ionization source, connected to the DMA P5. The exit of the DMA P5 was connected to a Lynx E11 electrometer and to an API-ToF-MS (TOFWERK AG, Switzerland), th~~o~~rough a customized interface (MION, Valladolid, Spain). API-ToF-MS has a very low background noise level and detection limit (< 1 ion/cm^3, Junninen et al., 2010). Moreover, both Api-TOF and Api-TOF coupling with a chemical ionization source (CI-API-TOF) have been successfully applied for atmospheric cluster measurement in laboratory and field, exhibiting the capability of detecting different atmospheric clusters, such as cluster complexes of sulfuric acid with ammonia (Kirkby et al., 2011; Lehtipalo et al., 2016), amine (Almeida et al., 2013; Yin et al., 2021), and organics (Riccobono et al., 2014). By the combination of API-TOF and DMA-P5, it is also possible to study the physiochemical properties of the atmospheric relevant clusters by scanning the electric field strength within the transfer optics (Lopez-Hilfiker et al., 2016). 200 mM sulfuric acid solution in 1:4 methanol/water mixture was used to generate negatively charged sulfuric acid clusters by ESI. The generation procedure was the same as the former sections. The mobility of sulfuric acid clusters was calibrated before each experiment with THA^+. Hereafter the bisulfate ions (HSO_4^-), negatively charged sulfuric acid dimers ($H_2SO_4HSO_4^-$), trimers

345 (($H_2SO_4)_2HSO_4^-$) and tetramers (($H_2SO_4)_3HSO_4^-$) are referred as sulfuric acid monomer $(SA)_1^-$, dimer $(SA)_2^-$, trimer $(SA)_3^-$ and tetramer $(SA)_4^-$, respectively.

Table 1 mobilities 1/Z (V $s^{-1}cm^{-2}$) and mobility diameter (nm) of sulfuric acid clusters

$Peak^+$	1/Z	Diameter
$(SA)_1^-$	0.497	1.02
$(SA)_2^-$	0.502	1.024
$(SA)_3^-$	0.589	1.111
$(SA)_4^-$	0.676	1.191

The ion mobility spectrum and ion mobility-mass to charge ratio 2D distribution (DMA-MS spectrum) are shown in Fig 9.
350 The multi-peak fitting analysis of the ion mobility spectrum (Fig. 9a) was conducted with Igor Multi-peak Fitting package. The fitted peaks were then identified with the DMA-MS spectrum. Well separated $(SA)_3^-$ and $(SA)_4^-$ peaks were observed. Due to insufficient resolution, $(SA)_1^-$ and $(SA)_2^-$ were not separated within the ion mobility spectrum. The ion mobility (diameter) of $(SA)_1^-$ and $(SA)_2^-$ were obtained thorough DMA-MS spectrum. Table 1 shows the ion mobility and diameter of sulfuric acid monomer and larger clusters. The measured diameter of $(SA)_3^-$ was 1.11 nm, showed high consistency with the
355 reported value (Passananti et al., 2019). Since the voltage configurations can affect the fragmentation of the cluster inside the API-ToF-MS (Passananti et al., 2019), the DMA-MS spectrum is highly instrument dependent. Cautions should be paid on the comparison between different experiments. Given that the clusters forming as precursors to atmospheric nucleation are physically bound and often labile, the important issue arises as to whether the clusters observed in the mobility and the mass analyser are the original species present in the atmosphere, or rather their fragmentation products artificially generated during
360 the transfer to the vacuum system. The situations are even more complicated if fragmentation arise prior to or during the mobility measurements. Therefore, it is important to consider the fragmentation when interpreting the DMA-MS measurements. Ions with smaller mass but appearing at the same mobility of parent ions are originated from dissociation or decomposition. Under the condition that not all parent ions are fragmented into smaller ions within the mass analyser, we can determine which ions detected are the original ions selected in the DMA, and which are fragments. As shown in Fig. 9b, except for SA multimers,
365 cluster of methyl sulfate with $(SA)_1^-$ ($CH_4SO_4HSO_4^-$) was observed at the different mobility (V_{DMA} of about 1800 V and 2250 V). Cluster of ammonia molecule adducted on $(SA)_4^-$ was also identified at V_{DMA} of about 2450V. The first three peaks identified in the mobility spectrum (Fig 9a) were NO_2^-, CO_3^- and CHO_4^-. To further interpret the fragmentation, the ion mobility spectrum at the mass to charge ratio of the main observed ions/cluster-ion adducts was discussed (Fig S9): both $(SA)_1^-$ and $CH_3SO_4^-$ showed two peaks, with the latter one being fragments originated from $CH_4SO_4HSO_4^-$. The mobility of $(SA)_1^-$
370 and $(SA)_2^-$ was close, making the separation of $(SA)_1^-$ and $(SA)_2^-$ fragments difficult. Hower, it is unlikely that $(SA)_2^-$ fragmented contributed largely to $(SA)_1^-$, due to an obvious difference in central mobility. The latter two peaks of $(SA)_2^-$ were the fragments from $(SA)_3^-$ and cluster of methyl sulfate with $(SA)_2^-$ ($CH_4SO_4(H_2SO_4)HSO_4^-$). $(SA)_4^-$ would fragment into

$(SA)_3^-$ via losing one sulfuric acid molecule and originate from the fragmentation of NH_3-$(SA)_4^-$ and larger clusters. Under our experimental configuration, the interference of fragmentation on the intensity of SA clusters is minor (<10%). When the (CI)-API-TOF was deployed for atmospheric measurements, the instrument configuration should be checked by using similar experimental set up to avoiding underestimate of the clusters due to large de-cluster ratio.

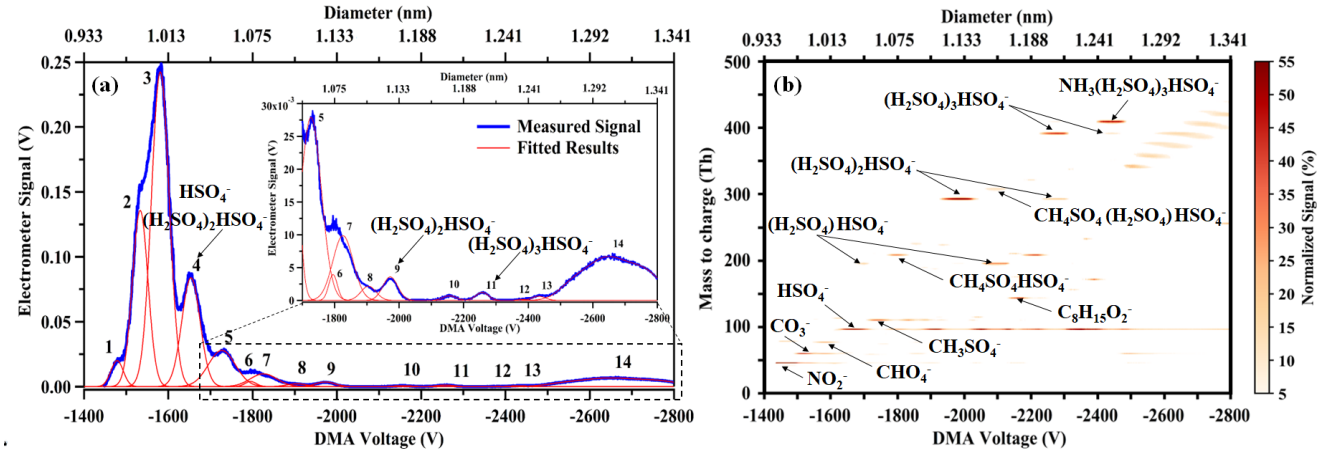

Fig. 9 Negative ion mobility spectrum of electrosprayed sulfuric acid of (a) electrometer and (b) DMA P5 coupled to API-ToF-MS. The signal of DMA-MS spectrum within each ion mobility step (V_{DMA} increased with the stepwise of 0.5V) is normalized to the total signal intensity of the corresponding ion mobility step.

4 Conclusions and Recommendations

We present the characterization results of a planar DMA (DMA P5) ~~with a home made recirculation system~~. ~~With this recirculation system, t~~The sizing range of DMA P5 is ~~0~~ sub 3.9 nm. Two operation modes can be applied (suction mode and counter flow mode). Under suction mode, the maximum resolving power can reach 60, while under counter flow mode, the maximum resolving power is 84~~, much closer to the theoretical limit~~. The resolving power of DMA P5 ~~is~~ can be ~~7~~5-16 times higher than commercial DMAs. Under suction mode, the obtained monodispersed aerosol number concentration can be modified by changing the injection flow rate. Under counter flow mode, although the resolving power is higher than the suction mode, the obtained monodispersed aerosol number concentration is lower due to the absence of injection flow. The ion transmission of DMA P5, tested by a TDMA system, exceeds 54.3%, which is about 7-8 times higher than commercial DMA (TSI 3086).

The application of DMA P5 was also characterized. Positive and negative aerosol ions of four tetra alkyl ammonium halides (THAB, TMAI, TBAI and TDAB) were measured, and high-resolution ion spectra were obtained. Finally, P5 was combined with an API-TOF-MS to successfully measure the two-dimensional (mass to charge ratio V.S. ion mobility) distribution of sulfuric acid clusters. The mobility diameters of sulfuric acid clusters (monomer to tetramer) were measured.

This system can be used to simultaneously measure the ion mobility and chemical composition of atmospheric clusters. In addition, this system can also be applied to calibrate the mass dependent ion transmission efficiency of mass spectrometry and study the impact of the collision induced cluster fragmentation (CICF) inside the mass spectrometry on the measurement results of atmospheric clusters.

Data Availability

Data available on request from the authors.

Conflicts of Interest

The authors declare no conflict of interests.

Author Contributions

Zhengning Xu: Methodology, System set up, Experiment, Formal analysis, Visualization, Writing Original draft, Review and editing. **Jian Gao, Zhuanghao Xu:** Experiment, System set up and Data curation. **Michel Attoui, Xiangyu Pei:** System set up, Review and editing. **Mario Amo-González, Kewei Zhang:** System set up. **Zhibin Wang:** Conceptualization, Project administration, Review and editing; Funding acquisition.

Acknowledgments

The research was supported by National Natural Science Foundation of China (NSFC) (42005086, 41805100, 91844301), the Fundamental Research Funds for the Central Universities (226-2023-00077) and the Key Research and Development Program of Zhejiang Province (2021C03165 and 2022C03084).

References

Ahonen, L., Li, C., Kubecka, J., Iyer, S., Vehkamaki, H., Petaja, T., Kulmala, M., and Hogan, C. J.: Ion mobility-mass spectrometry of iodine pentoxide-iodic acid hybrid cluster Anions in dry and humidified atmospheres, J. Phys. Chem. Lett. 10 (8), 1935–1941, https://doi.org/10.1021/acs.jpclett.9b00453, 2019.

Amo-González, M. and Pérez, S.: Planar Differential Mobility Analyzer with a Resolving Power of 110, Analytical Chemistry, 90, 6735-6741, 2018.

Almeida, J., Schobesberger, S., Kurten, A., Ortega, I. K., Kupiainen-Maatta, O., Praplan, A. P., et al.: Molecular understanding of sulphuric acid-amine particle nucleation in the atmosphere. Nature 502 (7471), 359–363. doi:10.1038/nature12663, 2013.

Amo- González, M., and Fernández de la Mora, J.: Mobility peak tailing reduction in a differential mobility analyzer (DMA) coupled with a mass spectrometer and several ionization sources, J. Am. Soc. Mass Spectrom. 28 (8),1506–1517, https://doi.org/10.1007/s13361-017-1630-2, 2017.

Attoui, M., M. Paragano, J. Cuevas, and J. Fernandez de la Mora.: Tandem DMA generation of strictly monomobile 1–3.5nm particle standards, Aerosol Sci. Technol. 47 (5):499–511, 2013.

Attoui, M. and Fernandez de la Mora, J.: Flow driven transmission of charged particles against an axial field in antistatic tubes at the sample outlet of a Differential Mobility Analyzer, Journal of Aerosol Science, 100, 91-96, 2016.

Cai, R.; Chen, D.-R.; Hao, J.; Jiang, J.: A miniature cylindrical differential mobility analyzer for sub-3 nm particle sizing, Journal of Aerosol Science, 106, 111-119, 2017.

Cai, R.; Attoui, M.; Jiang, J.; Korhonen, F.; Hao, J.; Petäjä, T.; Kangasluoma, J.: Characterization of a high-resolution supercritical differential mobility analyzer at reduced flow rates, Aerosol Science and Technology, 52, (11), 1332-1343, 2018.

Chen, D.-R., Pui, D. Y. H., Hummes, D., Fissan, H., Quant, F. R., and Sem, G. J.: Design and Evaluation of a Nanometer Aerosol Differential Mobility Analyzer (Nano-DMA), J. Aerosol Sci., 29(5):497–509. http://doi.org/10.1016/S0021-8502(97)10018-0, 1998.

Chen, Y., Wang, W., Liu, M., and Ge, M.: Measurement technologies of nanoparticle chemical composition and their application, J. Atmos. Environ. Opt. 15 (6), 402–412 , http://doi.org/10.3969/j.issn.1673-6141.2020.06.001,2020

Criado-Hidalgo, E., Fernandez-Garcia, J., and Fernandez de la Mora, J.: Mass and charge distribution analysis in negative electrosprays of large polyethylene glycol chains by ion mobility mass spectrometry, Anal. Chem. 85 (5), 2710–2716, http://doi.org/10.1021/ac303054x, 2013.

Fernandez de la Mora, J.: Space charge effects in ion mobility spectrometry, J. American Society Mass Spectrometry, 30(6), 1082-1091, 2019.

Fernandez de la Mora, J.; Bruce Thomson and M. Gamero-Castaño: Tandem mobility mass spectrometry study of electrosprayed Heptyl4N+Br- clusters, J. Am. Soc. Mass Spectrom., 16 (5): 717-732, 2005.

Fernández de la Mora, J., and Kozlowski, J.: Handheld differential mobility analyzers of high resolution for 1–30nm particles: Design and fabrication considerations, J. Aerosol Sci. 57:45–53, 2013.

Fernández de la Mora, J., Perez-Lorenzo, L. J., Arranz, G., Amo- González, M., and Burtscher, H.: Fast high-resolution nanoDMA measurements with a 25 ms response time electrometer, Aerosol Sci. Technol., 51, (6), 724-734, 2017.

Flagan, R. C.: On differential mobility analyzer resolution, Aerosol Sci. Technol. 30 (6):556–70, 1999.

Gao, J., Xu, Z., Cai, R., Skyttä, A., Nie, W., Gong, X., Zhu, L., Cui, S., Pei, X., Kuang, B., Kangasluoma, J., Wang, Z.: Molecular identification of organic acid molecules from α-pinene ozonolysis. Atmospheric Environment, 312, 2023.

Hogan, C. J., Jr., and Fernandez de la Mora, J.: Tandem ion mobility mass spectrometry (IMS-MS) study of ion evaporation from ionic liquidacetonitrile nanodrops, Phys. Chem. Chem. Phys. 11 (36), 8079–8090, http://doi.org/10.1039/b904022f, 2009.

Hogan, C. J., Jr., and Fernandez de la Mora, J.: Ion-pair evaporation from ionic liquid clusters, J. Am. Soc. Mass Spectrom. 21 (8), 1382–1386, http://doi.org/10.1016/j.jasms.2010.03.044, 2010.

Hogan, C. J., Jr., Ruotolo, B. T., Robinson, C. V., and Fernandez de la Mora, J.: Tandem differential mobility analysis-mass spectrometry reveals partial gas-phase collapse of the GroEL complex, J. Phys. Chem. B 115 (13), 3614–3621, http://doi.org/10.1021/jp109172k, 2011.

Javaheri, H., Le Blanc, Y., Thomson, B. A., de la Fernandez Mora, J., Rus, J., Sillero-Sepúlveda, J.A.: Evaluation of the analytical characteristic of a differential mobility analyzer coupled to a triple quadrupole system (DMA-MSMS), Poster 061, Annual meeting of the ASMS, June 1-5, Denver, CO, 2008.

Jiang, J., Chen, M., Kuang, C., Attoui, M., & McMurry, P. H.: Electrical mobility spectrometer using a diethylene glycol condensation particle counter for measurement of aerosol size distributions down to 1 nm, Aerosol Science and Technology, 45, 510–521, 2011.

Jiang, J., Attoui, M., Heim, M., Brunelli, N. A., McMurry, P. H., Kasper, G., Flagan, R. C., Giapis, K., and Mouret, G.: Transfer Functions and Penetrations of Five Differential Mobility Analyzers for Sub-2 nm Particle Classification, Aerosol Science and Technology, 45, (4), 480-492, 2011.

Junninen, H., Ehn, M., Petaja, T., Luosuarvi, L., Kotiaho, T., Kostiainen, R., Rohner, U., Gonin, M., Fuhrer, K., Kulmala, M., and Worsnop, D. R.: A high-resolution mass spectrometer to measure atmospheric ion composition, Atmos. Meas. Tech., 3, 1039–1053, doi:10.5194/amt-3-1039-2010, 2010.

Kerminen, V.-M., Chen, X., Vakkari, V., Petäjä, T., Kulmala, M. and Biachi, F.: Atmospheric new particle formation and growth: review of field observations, Environ. Res. Lett., http://doi.org/10.1088/1748-9326/aadf3c, 2018.

Knutson, E. O., & Whitby, K. T.: Aerosol classification by electric mobility: Apparatus, theory, and applications, Aerosol Science and Technology, 6, 443–451, 1975.

Kirkby, J., Curtius, J., Almeida, J., Dunne, E., Duplissy, J., Ehrhart, S., et al.: Role of sulphuric acid, ammonia and galactic cosmic rays in atmospheric aerosol nucleation. Nature 476 (7361), 429–433. doi:10.1038/nature10343, 2011.

Kulmala, M., Pirjola, L., Mäkelä, J. M.: Stable sulphate clusters as a source of new atmospheric particles, Nature, 404, (6773), 66-69, 2000.

Lehtipalo, K., Rondo, L., Kontkanen, J., Schobesberger, S., Jokinen, T., Sarnela, N., et al.: The effect of acid-base clustering and ions on the growth of atmospheric nano-particles. Nat. Commun. 7, 11594. doi:10.1038/ncomms11594, 2016.

Li, C. X., and Hogan, C. J.: Vapor specific extents of uptake by nanometer scale charged particles. Aerosol Sci. Technol. 51 (5), 653–664, http://doi.org/10.1080/02786826.2017.1288285, 2017.

Liu, Y., Attoui, M., Chen, J., Li, Q. and Wang, L.: Performance comparison of SMPSs with soft X-ray and Kr-85 neutralizers in a humid atmosphere, Journal of Aerosol Science, 154, 2021.

Lopez-Hilfiker, F. D., Iyer, S., Mohr, C., Lee, B. H., D'Ambro, E. L., Kurtén, T., and Thornton, J. A.: Constraining the sensitivity of iodide adduct chemical ionization mass spectrometry to multifunctional organic molecules using the collision limit and thermodynamic stability of iodide ion adducts, Atmos. Meas. Tech., 9, 1505–1512, https://doi.org/10.5194/amt-9-1505-2016, 2016.

May, J. C., & McLean, J. A.: Ion mobility-mass spectrometry: time-dispersive instrumentation. Anal Chem, 87 (3), 1422-36, 2015.

Oberreit, D., Rawat, V. K., Larriba-Andaluz, C., Ouyang, H., McMurry, P. H., and Hogan, C. J.: Analysis of heterogeneous water vapor uptake by metal iodide cluster ions via differential mobility analysis-mass spectrometry, J. Chem. Phys. 143 (10), 104204. http://doi.org/10.1063/1.4930278, 2015.

Oberreit, D. R., McMurry, P. H., and Hogan, C. J.: Analysis of heterogeneous uptake by nanoparticles via differential mobility analysis-drift tube ion mobility spectrometry, Phys. Chem. Chem. Phys. 16 (15), 6968–6979, http://doi.org/10.1039/c3cp54842b, 2014

Ouyang, H., He, S., Larriba-Andaluz, C., and Hogan, C. J.: IMS-MS and IMS-IMS investigation of the structure and stability of dimethylamine-sulfuric acid nanoclusters, J. Phys. Chem. A 119 (10), 2026–2036, http://doi.org/10.1021/jp512645g, 2015.

Passananti, M., Zapadinsky, E., Zanca, T., Kangasluoma, J., Myllys, N., Rissanen, M. P., Kurten, T., Ehn, M., Attoui, M., Vehkamaki, H.: How well can we predict cluster fragmentation inside a mass spectrometer? Chem Commun (Camb), 55, (42), 5946-5949, 2019.

Peng, C., Deng, C., Lei, T., Zheng, J., Zhao, J., Wang, D., Wu, Z., Wang, L., Chen, Y., Liu, M, Jiang, J., Ye, A., Ge, M., Wang, W.: Measurement of atmospheric nanoparticles: Bridging the gap between gas-phase molecules and larger particles, J. Environ. Sci, http://doi.org/10.1016/j.jes.2022.03.006, 2022.

Perraud, V., Li, X. X., Jiang, J. K., Finlayson-Pitts, B. J., and Smith, J. N.: Size-resolved chemical composition of sub-20 nm particles from methanesulfonic acid reactions with methylamine and ammonia, ACS Earth Space Chem. 4 (7), 1182–1194, http://doi.org/10.1021/acsearthspacechem.0c00120, 2020.

Purves, R. W., Guevremont, R., Day, S., Pipich, C. W., and Matyjaszczyk, M. S.: Mass spectrometric characterization of a high-field asymmetric waveform ion mobility spectrometer, Rev. Sci. Instrum., 69, 4094−4104, http://doi.org/10.1063/1.1149255, 1998.

Riccobono, F., Schobesberger, S., Scott, C. E., Dommen, J., Ortega, I. K., Rondo, L., et al.: Oxidation products of biogenic emissions contribute to nucleation of atmospheric particles. Science 344 (6185), 717–721. doi:10.1126/science.1243527, 2014.

Rioseras, A.T., Gaugg, M.T., Martinez-Lozano Sinues, P.: Secondary electrospray ionization proceeds via gas-phase chemical ionization. Anal. Methods 9, 5052–5057, 2017.

Rus, J., Moro, D., Sillero, J. A., Royuela, J., Casado, A., Estevez-Molinero, F., and Fernández de la Mora, J.: IMS–MS studies based on coupling a differential mobility analyzer (DMA) to commercial API–MS systems. Int. J. Mass Spectrom. 298 (1), 30–40, http://doi.org/10.1016/j.ijms.2010.05.008, 2010.

Smith, J. N., Moore, K. F., McMurry, P. H., and Eisele, F. L.: Atmospheric measurements of sub-20 nm diameter particle chemical composition by thermal desorption chemical ionization mass spectrometry, Aerosol Sci. Technol. 38 (2), 100–110, http://doi.org/10.1080/02786820490249036, 2004.

Steiner, G., Jokinen, T., Junninen, H., Sipila, M., Petaja, T., Worsnop, D., Reischl, G., Kulmala, M., High-Resolution Mobility and Mass Spectrometry of Negative Ions Produced in a Am241 Aerosol Charger, Aerosol Sci. & Techn. 48(3) 261-270, 2014.

Stolzenburg, M., Scheckman, J., Attoui, M., Han, H., and McMurry, P.: Characterization of the TSI model 3086 differential mobility analyzer for classifying aerosols down to 1 nm, Aerosol Science and Technology, 52:7, 748-756, http://doi.org/10.1080/02786826.2018.1456649, 2018.

Tammet, H.: SIZE AND MOBILITY OF NANOMETER PARTICLES, CLUSTERS AND IONS, J. Aerosol Sci., 6, (3), 459-475, https://doi.org/10.1016/0021-8502(94)00121-E, 1995.

Tauber, C., Chen, X., Wagner, P.E., Winkler, P.M., Hogan C.J., Maißer, A.: Heterogeneous nucleation onto monoatomic ions: support for the Kelvin-Thomson theory, ChemPhysChem 19 3144–3149, 2018.

Thomas, J. M., He, S., Larriba-Andaluz, C., DePalma, J.W., Johnston, M. V., and Hogan, C. J.: Ion mobility spectrometry-mass spectrometry examination of the structures, stabilities, and extents of hydration of dimethylamine-sulfuric acid clusters, Phys. Chem. Chem. Phys., 18, (33), 22962–22972, http://doi.org/10.1039/c6cp03432b, 2016.

Ude, S. , Fernandez de la Mora, J., Thomson, B. A.: Charge-induced unfolding of multiply charged polyethylene glycol ions, J. Am. Chem. Soc., 126, 12184-12190, 2004.

Ude, S. and Fernández de la Mora, J.: Molecular monodisperse mobility and mass standards from electrosprays of tetra-alkyl ammonium halides, J. Aerosol Sci., 36, (10), 1224-1237,2005.

Wiedensohler, A., Birmili, W., Nowak, A., Sonntag, A., Weinhold, K., Merkel, M., et al.: Mobility particle size spectrometers: harmonization of technical standards and data structure to facilitate high quality long-term observations of atmospheric particle number size distributions, Atmos. Meas. Tech., 5, (3), 657-685, 2012.

Yin, R., Yan, C., Cai, R., Li, X., Shen, J., Lu, Y., et al.: Acid-base clusters during atmospheric new particle formation in urban beijing. Beijing: Environmental Science & Technology. doi:10.1021/acs.est.1c02701, 2021.

Zhang, K., Xu, Z., Gao, J., Xu, Z., and Wang, Z.: Review of online measurement techniques for chemical composition of atmospheric clusters and sub-20nm particles, Frontiers in Environmental Science, 10, 2022.